

THE ENVIRONMENT OF LOCAL ULTRALUMINOUS INFRARED GALAXIES

B. A. ZAUDERER,¹ S. VEILLEUX,¹ AND H. K. C. YEE²

Received 2006 August 1; accepted 2007 January 4

ABSTRACT

The spatial cluster-galaxy correlation amplitude, B_{gc} , is computed for a set of 76 $z < 0.3$ ultraluminous infrared galaxies (ULIRGs) from the 1 Jy sample. The B_{gc} parameter is used to quantify the richness of the environment within 0.5 Mpc of each ULIRG. We find that the environment of local ULIRGs is similar to that of the field with the possible exceptions of a few objects with environmental densities typical of clusters with Abell richness classes 0 and 1. No obvious trends are seen with redshift, optical spectral type, infrared luminosity, or infrared color (f_{25}/f_{60}). We compare these results with those of local AGNs and QSOs at various redshifts. The 1 Jy ULIRGs show a broader range of environments than local Seyferts, which are exclusively found in the field. The distribution of ULIRG B_{gc} -values overlaps considerably with that of local QSOs, consistent with the scenario where some QSOs go through a ultraluminous infrared phase. However, a rigorous statistical analysis of the data indicates that these two samples are not drawn from the same parent population. The B_{gc} distribution of QSOs shows a distinct tail at high B_{gc} -values, which is not apparent among the ULIRGs. This difference is consistent with the fact that some of the QSOs used for this comparison have bigger and more luminous hosts than the 1 Jy ULIRGs.

Subject headings: galaxies: active — galaxies: clusters: general — quasars: general

Online material: color figures

1. INTRODUCTION

Ultraluminous infrared galaxies (ULIRGs) are defined as galaxies with $L_{\text{IR}} = L(8\text{--}1000 \mu\text{m}) \geq 10^{12} L_{\odot}$ (see reviews by Sanders & Mirabel 1996; Lonsdale et al. 2006). This luminosity limit is roughly equivalent to the minimum bolometric luminosity of QSOs. At luminosities above $10^{12} L_{\odot}$, the space density of ULIRGs in the local universe is greater than that of optically selected quasars with similar bolometric luminosities by a factor of ~ 1.5 . Thus local ULIRGs represent the most common type of ultraluminous galaxy. Systematic optical and near-infrared imaging surveys have revealed that local ULIRGs are almost always undergoing major mergers (e.g., Surace & Sanders 1999; Surace et al. 2001; Scoville et al. 2000; Veilleux et al. 2002, 2006). Most of the gas and star formation (and AGN) activity in these systems are concentrated well within the central kiloparsec (e.g., Downes & Solomon 1998; Soifer et al. 2000, 2001). Ground-based optical and near-infrared spectroscopic studies of these objects have shown that at least 25%–30% of them show genuine signs of AGN activity (e.g., Kim et al. 1998; Veilleux et al. 1999a, 1997, 1999b). This fraction increases to $\sim 50\%$ among the objects with $\log [L_{\text{IR}}/L_{\odot}] \gtrsim 12.3$. These results are compatible with those from mid-infrared spectroscopic surveys (e.g., Genzel et al. 1998; Lutz et al. 1998, 1999; Rigopoulou et al. 1999; Tran et al. 2001).

ULIRGs are relevant to a wide range of astronomical issues, including the role played by galactic mergers in forming some or all elliptical galaxies (Genzel et al. 2001; Veilleux et al. 2002), the efficiency of transport of gas into the central regions of such mergers and the subsequent triggering of circumnuclear star formation (e.g., Mihos & Hernquist 1996; Barnes 2004), the resulting heating and metal enrichment of the IGM by galactic winds (e.g., Rupke et al. 2002, 2005a, 2005b; Veilleux et al. 2005;

Martin 2005), the potential growth and fueling of supermassive black holes and the possible origin of quasars (Sanders et al. 1988). The discovery of $z = 1\text{--}4$ submillimeter sources with SCUBA (e.g., Smail et al. 1997; Hughes et al. 1998) suggests that ULIRGs are also relevant to the dominant source of radiant energy in the universe today. Indeed, integration of the light from the SCUBA population shows that it may account for most of the submillimeter/far-infrared background, as a result of the strong cosmological evolution of these sources (e.g., Chapman et al. 2005). Thus, while the present-day ULIRGs provide a relatively small contribution to the total present background, their cousins at high z are fundamentally important in this regard.

If ULIRGs are the predecessors of QSOs, one would expect ULIRGs and QSOs to live in similar environments. Surprisingly little has been published on the environments of local ULIRGs, in stark contrast to the abundant literature on the small- and large-scale environments of AGNs and QSOs (e.g., Yee et al. 1986; Yee & Green 1987; Ellingson et al. 1991; Hill & Lilly 1991; de Robertis et al. 1998a, 1998b; McLure & Dunlop 2001; Wold et al. 2000, 2001; Barr et al. 2003; Miller et al. 2003; Kauffmann et al. 2004; Söchting et al. 2004; Wake et al. 2004; Croom et al. 2005; Waskett et al. 2005; Serber et al. 2006) and the growing literature on the environments of $z \gtrsim 1$ ULIRGs (e.g., Blain et al. 2004; Farrah et al. 2004, 2006). To our knowledge, Tacconi et al. (2002) is the only published study that has attempted to quantify the environments of local ULIRGs. They correlated the positions of local ULIRGs with the catalogs of galaxy clusters and groups available in NED and found that none of them are located within a galaxy cluster. The lack of a comprehensive imaging database at the time prevented them from carrying out a more quantitative clustering analysis of these objects.

The present paper remedies the situation by using the large imaging database of Veilleux et al. (2002) to quantify the environment of local ($\langle z \rangle \sim 0.15$) ULIRGs from the 1 Jy sample. We note that the spectroscopy portion of the Sloan Digital Sky Survey (SDSS) provides redshift information for only the bright tail of the galaxy luminosity function at $z \sim 0.15$, so a method that

¹ Department of Astronomy, University of Maryland, College Park, MD 20740; zauderer@mail.umd.edu, veilleux@astro.umd.edu.

² Department of Astronomy and Astrophysics, University of Toronto, Toronto, ON M5S 3H4, Canada; hyee@astro.utoronto.ca.

relies solely on the photometric measurements of the galaxies in the field surrounding the ULIRG must be used for the present analysis. The properties of the 1 Jy sample and imaging data set are reviewed in § 2. In § 3 the procedure for deriving the environmental richness, B_{gc} , is outlined. Results for our sample are presented in § 4. The findings of environmental studies for quasars and Seyferts are compared with our results in § 5. Our conclusions are summarized in § 6. We use $H_0 = 50 \text{ km s}^{-1} \text{ Mpc}^{-1}$, $\Omega_m = 1$, and $\Omega_\lambda = 0$ throughout this paper. These values were selected to match those of previous studies and facilitate comparisons; they have no effect on our conclusions.

2. SAMPLE

The *IRAS* 1 Jy sample of 118 ULIRGs identified by Kim & Sanders (1998) is the starting point of our investigation. The 1 Jy ULIRGs were selected to have high galactic latitude ($|b| \geq 30^\circ$), $60 \mu\text{m}$ flux greater than 1 Jy, $60 \mu\text{m}$ flux greater than their $12 \mu\text{m}$ flux (to exclude infrared-bright stars), and ratios of $60 \mu\text{m}$ flux to $100 \mu\text{m}$ flux above $10^{-0.3}$ (to favor the detection of high-luminosity objects).

All 1 Jy ULIRGs were imaged at optical (R) and near-infrared (K') wavelengths using the U . of Hawaii 2.2 m telescope. The present study uses only the R -band images since they have a larger field of view (FOV) and are deeper than the K' -band images. The R filter at 6400 \AA was a Kron-Cousins filter. Details of the observations and data reduction can be found in Kim et al. (2002). The analysis of these data is presented in Veilleux et al. (2002). These data are part of comprehensive imaging and spectroscopic surveys which also include a large set of optical and near-infrared spectra of the nuclear sources (Veilleux et al. 1999a, 1999b and references therein), a growing set of spatially resolved near-infrared spectra to study the gas and stellar kinematics of the hosts (Genzel et al. 2001; Tacconi et al. 2002; Dasyra et al. 2006a, 2006b), and mid-infrared spectra from the *Infrared Space Observatory (ISO)* and the *Spitzer Space Telescope (Spitzer)*; e.g., Genzel et al. 1998; S. Veilleux et al. 2007, in preparation). This effort is called QUEST (Quasar and ULIRG Evolutionary Study).

Since the set of data presented in Kim et al. (2002) was compiled from observations made over the course of 14 years, a variety of CCDs were used and the FOV sizes and spatial resolutions are not uniform. For consistency, we limit the set of data in this paper to the images of the 76 objects taken under good photometric conditions with the TEK 2048×2048 CCD. Of these images, 32 (42%) were irrecoverably cropped during an earlier stage of data reduction and have a significantly reduced FOV size. The effects of the cropping on the results of our analysis are discussed in § 4. Table 1 lists the objects in our sample along with the FOV size and several other properties of the sources.

3. ANALYSIS

In this section we explain the methods that we used to quantify the environment richness around each ULIRG. First, we describe the algorithms used to find objects in the field and identify them as stars or galaxies. Next we discuss the formalism applied to calculate the environment richness parameter, B_{gc} . The techniques used for our analysis have already been described in detail in Yee (1991), Ellingson et al. (1991), Yee & López-Cruz (1999), and Gladders & Yee (2005); here we highlight the main steps.

3.1. Object Identification and Classification

Object identification was accomplished using the Picture Processing Package (PPP) developed by one of us (Yee 1991). This program systematically examines each pixel in the image and

determines whether it has the potential to be part of an object: a star, a galaxy, a cosmic ray, or an artifact of the CCD. After running through a series of tests, the PPP object finding program identifies and catalogs the location and peak brightness of objects in the image. The algorithms used here are modified versions of that used by Kron (1980), which depend on searching for local maxima. They have been shown to be robust for object identification in sparse to moderately crowded fields (Yee 1991). The 1 Jy sample selection criterion $|b| \geq 30^\circ$ avoids extremely crowded fields (and reduces the effects of dust extinction on the galaxy counts), which could lead to object misclassification and erroneous environment richness measurements. We therefore find that this object finding routine is perfectly adequate for all ULIRGs in our sample.

To address the problem of bad pixels or cosmic rays, objects were thrown out automatically if a given pixel was 5 times brighter than those immediately surrounding it. This did not always work well because bright bad pixels are sometimes surrounded by other bad pixels. So some misidentified objects were also identified by eye and removed by hand.

The next step was to run an aperture photometry algorithm on the identified objects in each image to determine whether these objects are stars or galaxies. For each object, a growth curve was calculated using a series of circular apertures centered on the intensity centroid of the object. A reference-star growth curve was created for each quadrant of the CCD frame by averaging the growth curves of bright, isolated, and unsaturated stars within each quadrant. The growth curves of the other objects were then compared with the reference-star growth curve using the classification parameter C_2 defined by Yee (1991). In essence, C_2 computes the average difference per aperture between the growth curves of the objects and the growth curve of the reference star after they have been scaled to match at the center and effectively compares the ratio between the fluxes in the center and the outer part of an object with that of the reference star. This method has been thoroughly tested by Yee (1991); readers interested in knowing more about this classification scheme should refer to this paper for detail.

3.2. Environment Richness Parameter

We use the parameter B_{gc} to quantify the richness of the environment of ULIRGs. B_{gc} is the amplitude of the galaxy-galaxy correlation function calculated for each object of interest individually. It was first used by Longair & Seldner (1979) to measure the environment of radio galaxies using galaxy counts, and subsequently adopted in most studies of the environments of quasars and other active galaxies (e.g., Yee & Green 1984; Ellingson et al. 1991; de Robertis et al. 1998a, 1998b; McLure & Dunlop 2001; Wold et al. 2000, 2001; Barr et al. 2003; Waskett et al. 2005), and also used as a quantitative measurement of galaxy cluster richness (e.g., Andersen & Owen 1994; Yee & López-Cruz 1999). Yee & López-Cruz (1999) have demonstrated the robustness of the B_{gc} parameter when galaxies are counted to different radii and to different depth. Furthermore, measurements of the environmental richness based on the photometrically derived B_{gc} -values have been shown to be entirely consistent with measurements based on spectroscopic data. This was demonstrated by Yee & Ellingson (2003), who used the data from the Canadian Network for Observational Cosmology Cluster Redshift Survey (CNOC1) to compare B_{gc} -values derived from (1) photometric data with background subtraction, and (2) from properly weighted spectroscopy data to account for incompleteness. We describe briefly the procedure for deriving B_{gc} below.

TABLE 1
GALAXIES PROPERTIES

| Name (1) | l (2) | b (3) | z (4) | $\log(L_{\text{IR}}/L_{\odot})$ (5) | ST (6) | $\log(f_{25}/f_{60})$ (7) | B_{gc} (8) | 1σ (9) | Field (10) |
|-------------|------------|------------|------------|--|-----------|------------------------------|------------------------|------------------|---------------|
| F00091-0738 | 95.6 | -68.1 | 0.118 | 12.19 | H II | -1.08 | -80 | 97 | 1240 |
| F00188-0856 | 100.5 | -70.2 | 0.128 | 12.33 | L | -0.85 | -26 | 103 | 1330 |
| F00397-1312 | 113.9 | -75.6 | 0.261 | 12.90 | H II | -0.74 | 25 | 137 | 2220 |
| F00456-2904 | 326.4 | -88.2 | 0.110 | 12.12 | H II | -1.27 | -34 | 94 | 1220 |
| F00482-2721 | 49.4 | -89.8 | 0.129 | 12.00 | L | -0.80 | 45 | 111 | 1390 |
| F01004-2237 | 152.1 | -84.6 | 0.118 | 12.24 | H II | -0.54 | 34 | 103 | 1290 |
| F01166-0844 | 143.6 | -70.2 | 0.118 | 12.03 | H II | -1.01 | 70 | 109 | 1240 |
| F01199-2307 | 183.3 | -81.8 | 0.156 | 12.26 | H II | -1.00 | -26 | 112 | 1550 |
| F01298-0744 | 151.1 | -68.1 | 0.136 | 12.27 | H II | -1.11 | 34 | 112 | 1390 |
| F01355-1814 | 174.9 | -75.9 | 0.192 | 12.39 | H II | -1.07 | -61 | 121 | 720 |
| F01494-1845 | 184.3 | -73.6 | 0.158 | 12.23 | ... | -0.93 | -99 | 113 | 1620 |
| F01569-2939 | 225.6 | -74.9 | 0.141 | 12.15 | H II | -1.09 | -118 | 108 | 1430 |
| F02411+0353 | 168.2 | -48.6 | 0.144 | 12.19 | ... | -0.79 | 24 | 113 | 1450 |
| F02480-3745 | 243.1 | -63.0 | 0.165 | 12.23 | ... | -1.06 | -70 | 114 | 1680 |
| F03209-0806 | 192.0 | -49.3 | 0.166 | 12.19 | H II | -0.89 | -71 | 115 | 1620 |
| F03250+1606 | 168.7 | -32.4 | 0.129 | 12.06 | L | -0.96 | -137 | 103 | 1330 |
| Z03521+0028 | 188.4 | -38.0 | 0.152 | 12.45 | L | -1.10 | -203 | 111 | 1520 |
| F04074-2801 | 225.9 | -46.4 | 0.153 | 12.14 | L | -1.28 | 121 | 130 | 1520 |
| F04103-2838 | 226.9 | -45.9 | 0.118 | 12.15 | L | -0.53 | 31 | 103 | 1240 |
| F04313-1649 | 213.6 | -37.8 | 0.268 | 12.55 | ... | -1.16 | -17 | 135 | 2260 |
| F05020-2941 | 231.5 | -35.1 | 0.154 | 12.28 | L | -1.29 | 301 | 153 | 1530 |
| F05024-1941 | 220.1 | -32.0 | 0.192 | 12.43 | S2 | -0.88 | -25 | 121 | 1800 |
| F05156-3024 | 233.2 | -32.4 | 0.171 | 12.20 | S2 | -1.06 | -3 | 116 | 1660 |
| F08201+2801 | 195.3 | +31.3 | 0.168 | 12.23 | H II | -0.89 | -173 | 123 | 650 |
| F08474+1813 | 208.7 | +34.1 | 0.145 | 12.13 | ... | -0.83 | -36 | 181 | 580 |
| F08591+5248 | 165.4 | +41.0 | 0.158 | 12.14 | ... | -0.80 | 65 | 143 | 620 |
| F09039+0503 | 225.0 | +32.1 | 0.125 | 12.07 | L | -1.09 | -96 | 120 | 520 |
| F09539+0857 | 228.5 | +44.8 | 0.129 | 12.03 | L | -0.98 | -100 | 121 | 530 |
| F10035+2740 | 202.7 | +53.5 | 0.165 | 12.22 | ... | -0.83 | 414 | 198 | 650 |
| F10091+4704 | 169.9 | +53.2 | 0.246 | 12.67 | L | -1.17 | 678 | 319 | 860 |
| F10190+1322 | 227.2 | +52.4 | 0.077 | 12.00 | H II | -0.94 | 277 | 140 | 860 |
| F10485-1447 | 264.6 | +38.7 | 0.133 | 12.17 | L | -0.84 | -45 | 119 | 550 |
| F10594+3818 | 180.5 | +64.7 | 0.158 | 12.24 | H II | -0.93 | -11 | 125 | 620 |
| F11028+3130 | 196.5 | +66.6 | 0.199 | 12.32 | L | -1.05 | 2 | 131 | 740 |
| F11180+1623 | 235.9 | +66.3 | 0.166 | 12.24 | L | -0.80 | 119 | 156 | 650 |
| F11223-1244 | 272.6 | +44.7 | 0.199 | 12.59 | S2 | -0.98 | 35 | 136 | 740 |
| F11387+4116 | 164.6 | +70.0 | 0.149 | 12.18 | H II | -0.86 | 180 | 160 | 600 |
| Z11598-0112 | 278.6 | +59.0 | 0.151 | 12.43 | S1 | -0.80 | -21 | 111 | 1510 |
| F12032+1707 | 254.8 | +75.3 | 0.217 | 12.57 | L | -0.74 | -194 | 127 | 1970 |
| F12127-1412 | 283.4 | +62.0 | 0.133 | 12.10 | L | -0.81 | -121 | 117 | 550 |
| F12265+0219 | 290.8 | +62.4 | 0.159 | 12.73 | S1 | -0.36 | -6 | 149 | 1570 |
| F12359-0725 | 295.7 | +63.4 | 0.138 | 12.11 | L | -0.95 | 192 | 163 | 560 |
| F12447+3721 | 127.9 | +80.0 | 0.158 | 12.06 | H II | -1.02 | -103 | 122 | 620 |
| F13106-0922 | 311.9 | +52.9 | 0.174 | 12.32 | L | -1.32 | 102 | 131 | 1680 |
| F13218+0552 | 324.4 | +67.1 | 0.205 | 12.63 | S1 | -0.47 | 92 | 148 | 760 |
| F13305-1739 | 316.8 | +43.8 | 0.148 | 12.21 | S2 | -0.47 | -140 | 122 | 590 |
| F13335-2612 | 315.3 | +35.3 | 0.125 | 12.06 | L | -1.00 | -58 | 101 | 1300 |
| F13342+3932 | 88.2 | +74.6 | 0.179 | 12.37 | S1 | -0.61 | 140 | 159 | 690 |
| F13443+0802 | 339.6 | +66.6 | 0.135 | 12.15 | S2 | -1.13 | -1 | 106 | 1380 |
| F13454-2956 | 317.3 | +31.1 | 0.129 | 12.21 | S2 | -1.49 | 118 | 122 | 1330 |
| F13469+5833 | 109.1 | +57.2 | 0.158 | 12.15 | H II | -1.50 | -134 | 128 | 620 |
| F13509+0442 | 338.8 | +62.9 | 0.136 | 12.27 | H II | -0.83 | 162 | 159 | 560 |
| F14053-1958 | 326.4 | +39.1 | 0.161 | 12.12 | S2 | -0.86 | -42 | 123 | 630 |
| F14060+2919 | 44.0 | +73.0 | 0.117 | 12.03 | H II | -1.06 | -84 | 115 | 490 |
| F14121-0126 | 341.1 | +54.9 | 0.151 | 12.23 | L | -1.10 | -85 | 122 | 600 |
| F14197+0813 | 355.5 | +61.2 | 0.131 | 12.00 | - | -0.76 | -139 | 104 | 1350 |
| F14202+2615 | 35.1 | +69.6 | 0.159 | 12.39 | H II | -1.00 | 6 | 130 | 630 |
| F14252-1550 | 334.3 | +40.9 | 0.149 | 12.15 | L | -0.70 | 80 | 144 | 600 |
| F15043+5754 | 94.7 | +51.4 | 0.151 | 12.05 | H II | -1.16 | 251 | 179 | 600 |
| F15206+3342 | 53.5 | +56.9 | 0.125 | 12.18 | H II | -0.70 | 45 | 123 | 660 |
| F15225+2350 | 35.9 | +55.3 | 0.139 | 12.10 | H II | -0.86 | -64 | 120 | 570 |
| F15327+2340 | 36.6 | +53.0 | 0.018 | 12.17 | L | -1.12 | -8 | 103 | 90 |
| F17044+6720 | 98.0 | +35.1 | 0.135 | 12.13 | L | -0.55 | -73 | 106 | 1440 |
| F17068+4027 | 64.7 | +36.1 | 0.179 | 12.30 | H II | -1.04 | 1192 | 240 | 870 |
| F17179+5444 | 82.5 | +35.0 | 0.147 | 12.20 | S2 | -0.83 | -161 | 110 | 1540 |

TABLE 1—*Continued*

| Name (1) | l (2) | b (3) | z (4) | $\log(L_{\text{IR}}/L_{\odot})$ (5) | ST (6) | $\log(f_{25}/f_{60})$ (7) | B_{gc} (8) | 1σ (9) | Field (10) |
|-------------------|------------|------------|------------|--|-----------|------------------------------|------------------------|------------------|---------------|
| F21208–0519 | 47.3 | –35.9 | 0.130 | 12.01 | H II | –0.89 | 153 | 127 | 1340 |
| F21477+0502 | 62.5 | –35.6 | 0.171 | 12.24 | L | –0.85 | –76 | 116 | 1660 |
| F22491–1808 | 45.2 | –61.0 | 0.076 | 12.09 | H II | –1.00 | 46 | 119 | 440 |
| F22541+0833 | 81.2 | –44.6 | 0.166 | 12.23 | S2 | –0.82 | 73 | 126 | 1620 |
| F23060+0505 | 81.7 | –49.1 | 0.173 | 12.44 | S2 | –0.43 | –221 | 116 | 1670 |
| F23129+2548 | 97.4 | –32.0 | 0.179 | 12.38 | L | –1.35 | 133 | 137 | 1710 |
| F23233+2817 | 101.1 | –30.6 | 0.114 | 12.00 | S2 | –0.65 | –2 | 96 | 1250 |
| F23234+0946 | 90.9 | –47.4 | 0.128 | 12.05 | L | –1.29 | 46 | 111 | 1330 |
| F23327+2913 | 103.7 | –30.5 | 0.107 | 12.06 | L | –0.98 | 78 | 108 | 1150 |
| F23389+0300 | 91.2 | –55.2 | 0.145 | 12.09 | S2 | –0.55 | 167 | 134 | 1460 |
| F23498+2423 | 106.3 | –36.3 | 0.212 | 12.40 | S2 | –0.93 | 278 | 161 | 1930 |

NOTES.—Col. (1): name from the *IRAS* Faint Source Database. The prefix “Z” indicates the two objects not in the Faint Source Catalog. Col. (2): Galactic longitude. Col. (3): Galactic latitude. Col. (4): redshift from Kim & Sanders (1998). Col. (5): logarithm of the infrared (8–1000 μm) luminosity in units of solar luminosity computed using the flux in all four *IRAS* bands following the prescription of Kim & Sanders (1998). Col. (6): optical spectral type from Veilleux et al. (1999a). Col. (7): *IRAS* 25 to 60 μm flux ratio. Col. (8): environment richness parameter computed using PPP program, as described in § 3 of this paper, in $\text{Mpc}^{1.77}$. Col. (9): 1σ uncertainty on B_{gc} in $\text{Mpc}^{1.77}$. Col. (10): field size in kiloparsecs.

In order to determine the richness of the environment around a ULIRG, we need to count the number of galaxies within a spherical volume with radius, r , from the ULIRG of interest. However, we necessarily must begin with a two-dimensional image, which is a projection of this volume onto the sky plane. The number of galaxies in a solid angle $d\Omega$, at an angular distance θ from the object of interest is given by (Seldner & Peebles 1978)

$$N(\theta)d\Omega = N_g[1 + w(\theta)]d\Omega, \quad (1)$$

where N_g is the average surface density of galaxies and $w(\theta)$, the angular correlation function, can be expressed approximately as a power law,

$$w(\theta) = A_{\text{gc}}\theta^{1-\gamma}. \quad (2)$$

A_{gc} is a measure of the average enhancement of galaxies in angular area, and $\gamma \approx 1.77$ empirically. Integrating equation (2) within a circle with radius θ yields

$$A_{\text{gc}} = \frac{N_{\text{tot}} - N_{\text{bgc}}}{N_{\text{bgc}}} \frac{(3 - \gamma)}{2} \theta^{\gamma-1}, \quad (3)$$

where N_{tot} and N_{bgc} are the total numbers of galaxies and background galaxies, respectively, within an angular radius of θ .

Next, the two-dimensional parameters must be translated into three dimensions. The angular correlation function $w(\theta)$ is translated into the spatial correlation function, $\xi(r)$, which describes the number of galaxies in volume element dV at distance r from the object of interest. It can be shown that $\xi(r) = B_{\text{gc}}r^{-\gamma}$, where γ has the same value as in equation (3) and B_{gc} is the spatial correlation amplitude, a measure of the richness of the environment around the galaxy. Longair & Seldner (1979) have shown that

$$B_{\text{gc}} = \frac{A_{\text{gc}}n_{\text{bg}}(m)D^{\gamma-3}}{I_{\gamma}\Psi(m, z)}. \quad (4)$$

The constant I_{γ} is an integration constant that depends on γ (Groth & Peebles 1977). The value $n_{\text{bg}}(m)$ is the expected count per unit angular area of background galaxies brighter than apparent magnitude m , $\Psi(m, z)$ is the normalized integrated luminosity function of galaxies to apparent magnitude m , at redshift z of the cluster, and D is the angular diameter distance to the ULIRG

at redshift z . For our calculations, we used $\gamma = 1.77$, $I_{\gamma} = 3.78$, and the cosmological parameters $H_0 = 50 \text{ km s}^{-1} \text{ Mpc}^{-1}$, $\Omega_m = 1$, and $\Omega_{\Lambda} = 0$ to match those of previous papers. For Ψ and $n_{\text{bg}}(m)$, we use the luminosity function and background counts derived from the Red-Sequence Cluster Survey (RCS; e.g., Gladders & Yee 2005).

The uncertainty on B_{gc} is computed using the formula

$$\frac{\Delta B_{\text{gc}}}{B_{\text{gc}}} = \frac{(N_{\text{net}} + 1.3^2 N_{\text{bg}})^{1/2}}{N_{\text{net}}} \quad (5)$$

where N_{net} is the net counts of galaxies over the background counts, N_{bg} . This is a conservatively large error estimate as it includes the expected counting statistics in N_{net} and the expected dispersion in background counts. The factor 1.3^2 is included to account approximately for the additional fluctuation from the clustered (and hence non-Poissonian) nature of the background counts (discussed in detail in Yee et al. 1986). We follow the prescription of Yee & López-Cruz (1999) and integrate the luminosity function from approximately $M_R = -25$ to $M_R^* + 2$ (where $M_R^* \approx -22.3$ for our cosmology) to calculate the galaxy counts. This corresponds roughly to $R = 15$ – 20 for the galaxies in our sample ($\langle z \rangle \approx 0.15$). This range of integration was found by Yee & López-Cruz (1999) to reduce the sensitivity to small intrinsic variation of M^* and variations in the faint-end slopes of the cluster luminosity function. The B_{gc} parameter is computed over a radius $r = 500$ kpc, either directly from the data when $\text{FOV} \geq 1$ Mpc or extrapolated to this radius when $\text{FOV} < 1$ Mpc. This radius is selected to match that of previous studies. The B_{gc} parameter is not sensitive to this radius (Yee & López-Cruz 1999; see also § 4).

4. RESULTS

The spatial correlation amplitude parameter, B_{gc} , was computed for each of the 76 ULIRGs in our sample. The B_{gc} -values and associated 1σ uncertainties are listed for each object in Table 1. The average (median) value of B_{gc} and 1σ scatter around the mean for our sample of 76 ULIRGs is $\langle B_{\text{gc}} \rangle = 35 \pm 198 \text{ Mpc}^{1.77}$ ($-3 \text{ Mpc}^{1.77}$). For comparison, the B_{gc} -values of field galaxies and clusters of Abell richness class (ARC) 0–4 are ~ 67.5 , 600 ± 200 , 1000 ± 200 , 1400 ± 200 , 1800 ± 200 , and $2200 \pm 200 \text{ Mpc}^{1.77}$, respectively (the field B_{gc} -value is from Davis & Peebles 1983; the values for ARC 0–4 are from Yee & López-Cruz

TABLE 2
COMPARISONS WITH AGN AND QSO ENVIRONMENTAL STUDIES

| SAMPLE SET (1) | N (2) | $\langle z \rangle$ (3) | $\langle B_{gc} \rangle$ (4) | ERROR (5) | MEDIAN (6) | K-S TEST | | WILCOXON | | t -TEST | | F -TEST | |
|---|------------|----------------------------|---------------------------------|--------------|---------------|--------------------|------------------|--------------------|-------------------|---------------------|-------------------|---------------------|-------------------|
| | | | | | | P_{large} (7) | P_{all} (8) | P_{large} (9) | P_{all} (10) | P_{large} (11) | P_{all} (12) | P_{large} (13) | P_{all} (14) |
| 1 Jy ULIRGs (large FOV only) ^a | 44 | 0.152 | 4 ± 121 | ± 18 | -5 | 1.000 | 1.000 | 1.000 | 0.717 | 1.000 | 0.356 | 1.000 | <0.001 |
| 1 Jy ULIRGs (all) ^b | 76 | 0.151 | 35 ± 198 | ± 15 | -3 | 1.000 | 1.000 | 0.717 | 1.000 | 0.356 | 1.000 | <0.001 | 1.000 |
| de Robertis et al. (1998b)..... | 27 | 0.022 | 40 ± 64 | ± 13 | 27 | 0.031 | 0.020 | 0.067 | 0.113 | 0.166 | 0.901 | <0.001 | <0.001 |
| Yee & Green (1984), PG QSOs..... | 34 | 0.155 | 157 ± 208 | ± 28 | 134 | 0.001 | 0.001 | 0.459 | 0.001 | 0.001 | 0.004 | <0.001 | 0.024 |
| McLure & Dunlop (2001), entire sample..... | 44 | 0.194 | 365 ± 409 | ± 56 | 241 | <0.001 | <0.001 | <0.001 | <0.001 | <0.001 | <0.001 | <0.001 | 0.001 |
| McLure & Dunlop (2001), radio-quiet and radio-loud QSOs..... | 34 | 0.192 | 304 ± 355 | ± 61 | 218 | <0.001 | <0.001 | 0.797 | <0.001 | <0.001 | <0.001 | <0.001 | 0.216 |
| McLure & Dunlop (2001), radio-quiet QSOs..... | 21 | 0.174 | 326 ± 432 | ± 79 | 209 | <0.001 | <0.001 | 0.006 | 0.007 | <0.001 | <0.001 | <0.001 | 0.455 |
| Ellingson et al. (1991)..... | 63 | 0.435 | 121 ± 341 | ± 25 | 74 | 0.017 | 0.018 | 0.150 | 0.210 | 0.032 | 0.065 | <0.001 | <0.001 |
| Wold et al. (2001), model 1..... | 20 | 0.676 | 336 ± 343 | ± 42 | 203 | <0.001 | <0.001 | <0.001 | <0.001 | <0.001 | <0.001 | <0.001 | 0.512 |
| Wold et al. (2001), model 2..... | 20 | 0.676 | 212 ± 332 | ± 43 | 146 | 0.001 | 0.001 | 0.011 | 0.019 | 0.001 | 0.003 | <0.001 | 0.410 |
| Wold et al. (2001), model 3..... | 20 | 0.676 | 210 ± 365 | ± 43 | 129 | 0.012 | 0.021 | 0.055 | 0.079 | 0.001 | 0.005 | <0.001 | 0.740 |
| Barr et al. (2003)..... | 20 | 0.823 | 463 ± 677 | ± 143 | 347 | <0.001 | <0.001 | 0.001 | 0.002 | <0.001 | <0.001 | <0.001 | 0.001 |

NOTES.—Col. (1): sample set used for statistical comparison. Col. (2): number of objects in the sample. Col. (3): mean redshift of sample. Col. (4): mean B_{gc} -value and 1σ scatter around the mean of sample in $\text{Mpc}^{1.77}$. Col. (5): rms uncertainty on the mean of the B_{gc} -values in $\text{Mpc}^{1.77}$. Col. (6): median B_{gc} -value of sample in $\text{Mpc}^{1.77}$. Cols. (7) and (8): results from two-sided K-S test. Entries in col. (7) refer to comparison with the set of 44 ULIRGs that have an image size greater than $1 \text{ Mpc} \times 1 \text{ Mpc}$, while the entries in col. (8) refer to comparison with the entire set of 76 ULIRG images, regardless of field size. Cols. (9) and (10): results from Wilcoxon matched-pairs signed-ranks test. Entries in col. (9) refer to comparison with the set of 44 ULIRGs that have an image size greater than $1 \text{ Mpc} \times 1 \text{ Mpc}$, while the entries in col. (10) refer to comparison with the entire set of 76 ULIRG images, regardless of field size. Cols. (11) and (12): results from Student's t -test on the means of the distributions. Entries in col. (11) refer to comparison with the set of 44 ULIRGs that have an image size greater than $1 \text{ Mpc} \times 1 \text{ Mpc}$, while the entries in col. (12) refer to comparison with the entire set of 76 ULIRG images, regardless of field size. Cols. (13) and (14): results from an F -test on the standard deviations of the distributions. Entries in col. (13) refer to comparison with the set of 44 ULIRGs that have an image size greater than $1 \text{ Mpc} \times 1 \text{ Mpc}$, while the entries in col. (14) refer to comparison with the entire set of 76 ULIRG images, regardless of field size.

^a These entries refer to the 44 ULIRGs that have an image size greater than $1 \text{ Mpc} \times 1 \text{ Mpc}$.

^b These entries refer to the entire set of 76 ULIRG images, regardless of field size.

1999). The average clustering around the local ULIRGs therefore corresponds to an environment similar to the field. A large scatter is seen in our data: although most objects are consistent with no galaxy enhancement, a few objects apparently lie in clusters of Abell classes 0 and 1.

Before discussing the results any further, it is important to verify that our analysis of the cropped ($\text{FOV} < 1 \text{ Mpc}$) images does not introduce any bias when compared with the results from the uncropped ($\text{FOV} \geq 1 \text{ Mpc}$) images. The average (median) B_{gc} -value for the 44 objects with uncropped images is $4 \pm 121 \text{ Mpc}^{1.77}$ ($-5 \text{ Mpc}^{1.77}$); i.e., slightly smaller than the values found for the entire sample. Statistical tests give mixed results regarding the significance of this discrepancy (Table 2). The results from a two-sided Kolmogorov-Smirnov (K-S) test, a Wilcoxon matched-pairs signed-ranks test, and a Student's t -test on the means of the distributions suggest that the distribution of B_{gc} -values for the uncropped images is not significantly different from the distribution of B_{gc} -values as a whole, while the results from an F -test on the standard deviations of the distributions suggest a significant difference.

We have examined the distributions of B_{gc} -values for cropped and uncropped images as a function of Galactic latitudes and longitudes. Assuming that the B_{gc} -values are unaffected by stellar contaminants from our Galaxy, there should be no trend with Galactic latitude or longitude. Indeed, the distributions of B_{gc} -values with latitude and longitude are consistent with being random. Our data therefore confirm the results of Yee & López-Cruz (1999), who found that changing the counting radius by a factor of 2, both increasing to 1 Mpc and decreasing to 0.25 Mpc, did not alter the B_{gc} -values significantly. However, given the mixed results from the statistical tests, we track the cropped and uncropped data using different symbols in the various figures of this paper. We have verified that none of the results discussed below are af-

ected if the counting radius is chosen to be 0.25 or 1 Mpc rather than 0.50 Mpc, although quantization errors becomes noticeable when the counting radius is 0.25 Mpc due to poorer number statistics. A counting radius of 0.5 Mpc is adopted in the rest of this paper to match that of previous studies.

Next, we explore the possibility of a dependence of the environment richness on ULIRG properties. The first parameter we examine is the infrared luminosity (Fig. 1). Statistical tests indicate that no trend is present between B_{gc} and L_{IR} . This is true for both the uncropped data and the entire sample. The same result is found when we examine the environment richness as a function of redshift (Fig. 2). Here, however, the redshift range covered by our ULIRGs is very narrow ($z = 0.1-0.22$, if we exclude four objects in the sample), so this statement is not statistically very significant. Comparisons with the results of Blain et al. (2004) and Farrah et al. (2004, 2006) suggest that the environment of high- z ULIRGs is richer than that of local ULIRGs. We return to this point in § 5.

In Figure 2, we also distinguish between optical spectral types. We separate our sample into Seyfert 1s, Seyfert 2s, LINERs, and H II region-like galaxies based on the optical classification of Veilleux et al. (1999a). No obvious trends are observed with spectral type, but the subdivision of our sample into four subsets necessarily leads to poorer statistics. In Figure 3, we plot B_{gc} as a function of $\log(f_{25}/f_{60})$, another clear indicator of AGN activity [objects with $\log(f_{25}/f_{60}) > -0.7$ have “warm,” AGN-like $IRAS$ colors]. The lack of trends in this figure and Figure 2 indicates that the nature of the dominant energy source in local ULIRGs (starburst or AGN) is not influenced by the environment. This result is consistent with the ULIRG-QSO evolutionary scenario of Sanders et al. (1988), where the nature of the dominant energy source varies with merger phase (starburst in early phases and QSO in late phases) but is independent of the environment (as long as the

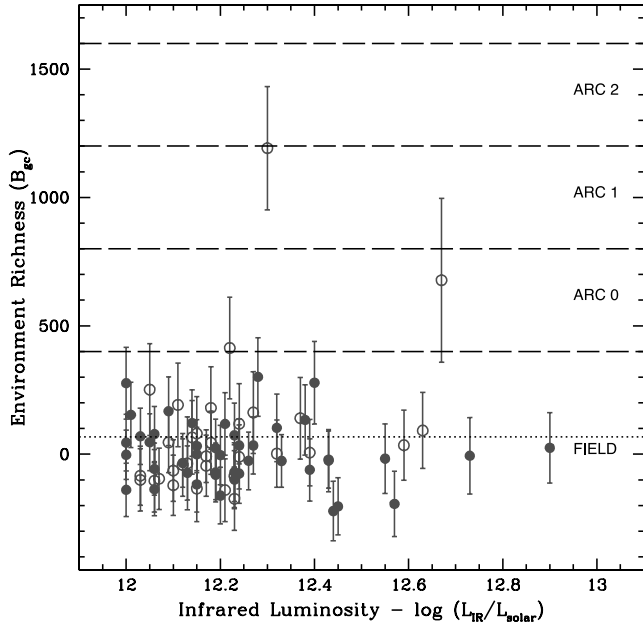


FIG. 1.—Environmental richness parameter vs. the infrared luminosity for local ULIRGs. Images that were cropped smaller than $1 \text{ Mpc} \times 1 \text{ Mpc}$ are noted by open circles, while the non-cropped images are shown as filled circles. The horizontal dashed line at $B_{gc} = 67.5 \text{ Mpc}^{1.77}$ indicates the average value for typical field galaxies. The range of environment richness parameters for the Abell richness classes are marked, following the definitions of Yee & López-Cruz (1999). No systematic trend is visible between environment richness and infrared luminosity. [See the electronic edition of the Journal for a color version of this figure.]

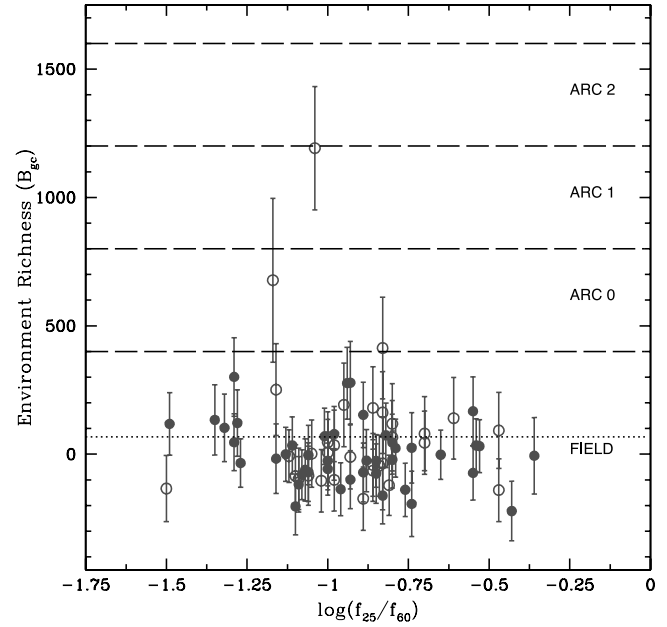


FIG. 3.—Environment richness parameter vs. the logarithm of the *IRAS* 25 to 60 μm flux ratio, $\log(f_{25}/f_{60})$, for local ULIRGs. ULIRGs with $\log(f_{25}/f_{60}) > -0.7$ are “warm” AGN-like systems. The meaning of the horizontal lines and symbols is the same as that in Fig. 1. No systematic trend is visible between environment richness and the 25 to 60 μm flux ratio. [See the electronic edition of the Journal for a color version of this figure.]

dispersion in velocity of the galaxies within the cluster is not too large to prevent mergers altogether).

5. COMPARISON WITH AGN SAMPLES

In this section we compare our results with those from published environmental studies of AGNs and QSOs. Table 2 summarizes the statistical results of these comparisons and Figures 4–9

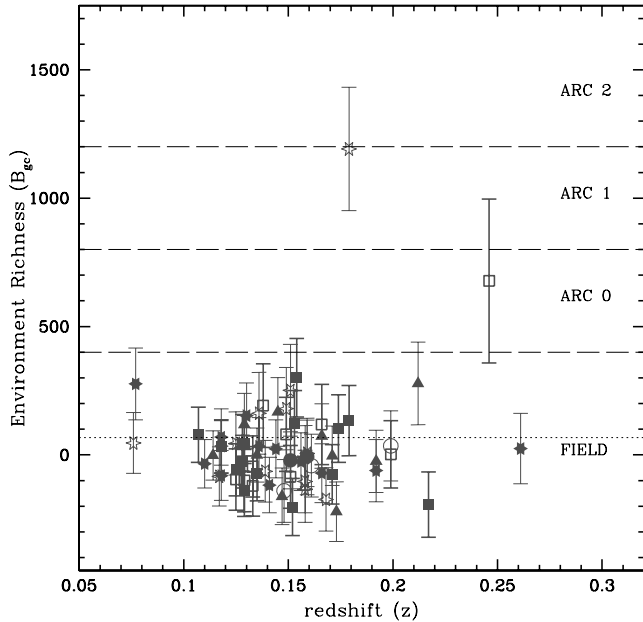


FIG. 2.—Environmental richness parameter vs. the redshift for local ULIRGs. The symbols reflect the optical spectral types of the ULIRGs, as listed in Veilleux et al. (1999a): circles are Seyfert 1 galaxies, triangles are Seyfert 2 galaxies, squares are LINERs, and stars are H II region-like galaxies. Open and filled symbols stand for cropped and uncropped images, respectively. The meaning of the horizontal lines is the same as that in Fig. 1. There are no statistically significant trends between environment richness and redshift or optical spectral type. [See the electronic edition of the Journal for a color version of this figure.]

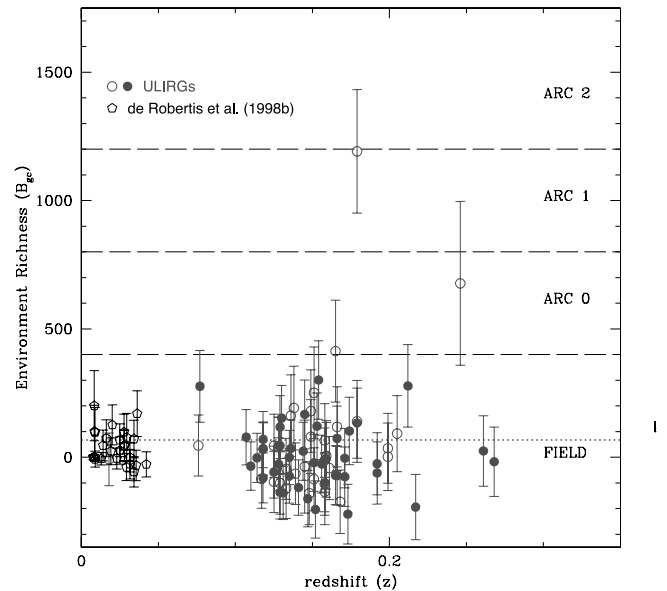


FIG. 4.—Comparison of the environment richness parameters for the local ULIRGs with those of $z < 0.05$ Seyfert galaxies from de Robertis et al. (1998b). The meaning of the horizontal lines and filled and open circles is the same as that in Fig. 1. Pentagons are the data from de Robertis et al. The B_{gc} distribution of local ULIRGs is distinctly broader than that of nearby Seyferts. [See the electronic edition of the Journal for a color version of this figure.]

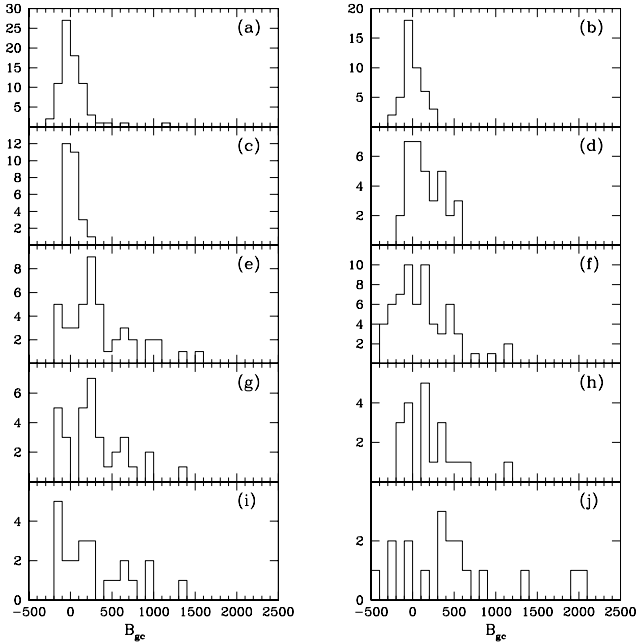


FIG. 5.—Histograms showing the distributions of environment richness parameters for (a) local ULIRGs from this paper (entire sample); (b) local ULIRGs from this paper (uncropped data only); (c) $z < 0.05$ Seyfert galaxies from de Robertis et al. (1998b); (d) $z \approx 0.2$ PG QSOs from Yee & Green (1984); (e) $z \approx 0.2$ QSOs and radio galaxies from McLure & Dunlop (2001); (f) $z \approx 0.2$ QSOs from McLure & Dunlop (2001); (g) $z \approx 0.2$ radio-quiet QSOs from McLure & Dunlop (2001); (h) $0.3 < z < 0.6$ radio-loud and radio-quiet QSOs from Ellingson et al. (1991); (i) $0.5 \leq z \leq 0.8$ radio-quiet QSOs from Wold et al. (2001; model 2 of the background galaxies); and (j) $0.6 < z < 1.1$ radio-loud QSOs from Barr et al. (2003). The results of statistical comparisons between these various data sets are listed in Table 2. None of these data sets appears to be drawn from the same parent population as the local ULIRGs, although considerable overlap in the values of the environmental richness parameters is seen between the various samples, particularly the local ULIRGs (this paper), local Seyferts (de Robertis et al. 1998b), and PG QSOs (Yee & Green 1984).

display the B_{gc} -values from the various samples. Unless otherwise noted in the text below, all data sets use the same cosmology.

5.1. Local Seyferts

First, we compare our results with those derived on nearby AGNs. De Robertis et al. (1998a, 1998b) studied the environments of nearby ($z < 0.05$) Seyfert galaxies using the exact same procedure as the one we use here, so we can directly compare their results with ours. For the 27 galaxies with $z > 0.0045$, de Robertis et al. (1998b) find $\langle B_{\text{gc}} \rangle = 40 \pm 63 \text{ Mpc}^{1.77}$ (median of $27 \text{ Mpc}^{1.77}$), consistent with the environment of field galaxies. Recent studies based on the SDSS database confirm this result (e.g., Miller et al. 2003; Wake et al. 2004). The average environment of local ULIRGs is therefore not dissimilar to that of local Seyferts. However, as indicated in Table 2, virtually all statistical tests except perhaps the t -test on the means indicate that the two B_{gc} distributions are not drawn from the same parent population. Figures 4 and 5 show why that is the case: The distribution of B_{gc} -values among ULIRGs is distinctly broader than that of the Seyferts. This slight difference is also seen in Figure 6, where we display the distribution of local Seyferts and local ULIRGs as a function of Abell richness classes.

As discussed in § 4, Seyfert-like ULIRGs do not reside in distinctly poorer or richer environments than non-Seyfert ULIRGs, so the broader scatter in ULIRG environments cannot be attributed to the broad range of AGN activity level within the ULIRG population. We note that typical error bars for the de Robertis et al.

(1998b) sample is $\sim 100 \text{ Mpc}^{1.77}$, while it is $\sim 150 \text{ Mpc}^{1.77}$ for the ULIRG sample. (The difference is due to the redshift difference between the samples—the ULIRG data requires counting to a fainter magnitude, which introduces larger uncertainties from background counts.) But the full ULIRG sample distribution is about 3 times broader than the Seyfert distribution—so, the broader distribution of the ULIRG sample cannot be fully explained by the larger error bars.

5.2. Local QSOs

Next, we compare our results with those derived on the nearby ($z \approx 0.2$) QSOs by Yee & Green (1984) and McLure & Dunlop (2001). The measurements of Yee & Green (1984) can be directly compared with our ULIRG results since their results were derived using the same method and parameters as that of the present study. McLure & Dunlop also apply the same formalism to calculate B_{gc} . However, they use a different analysis package to identify and classify the objects in the field and carry out the photometry. Their use of *HST* WFPC2 data also limits their survey area to only $\sim 200 \text{ kpc}$ around the QSOs, smaller than even our cropped data. These possible caveats should be kept in mind when comparing their results with ours.

Yee & Green (1984) get $\langle B_{\text{gc}} \rangle = 157 \pm 208$ and a median of $134 \text{ Mpc}^{1.77}$ for 34 QSOs from the Palomar-Green sample (Schmidt & Green 1983), while McLure & Dunlop (2001) derive an average (median) B_{gc} of $365 \pm 404 \text{ Mpc}^{1.77}$ ($241 \text{ Mpc}^{1.77}$) for a set of 44 radio-quiet and radio-loud QSOs and radio galaxies. If we limit our discussion to the QSOs in McLure & Dunlop sample (21 radio-quiet QSOs and 13 radio-loud QSOs), the average (median) B_{gc} becomes $304 \pm 350 \text{ Mpc}^{1.77}$ ($218 \text{ Mpc}^{1.77}$). The average environment of the QSOs in both studies is therefore slightly richer than that of local ULIRGs. The B_{gc} distributions of the two sets of local QSOs (particularly that of the McLure & Dunlop sample; see Fig. 5) show a distinct tail at high B_{gc} -values which is not apparent in the ULIRG distribution.

A quantitative analysis generally confirms that the B_{gc} distributions of Yee & Green and B_{gc} distributions for the radio-quiet and radio-loud QSOs from McLure & Dunlop are statistically different from that of the local ULIRGs (Table 2). However, note that the Wilcoxon test suggests that the difference is barely significant. Indeed, Figures 5, 7, and 8 show that there is considerable overlap between the B_{gc} distributions of 1 Jy ULIRGs and low- z QSOs, particularly the PG QSOs. This result is consistent with the idea that some, but perhaps not all, of these QSOs may have formed through a IR-luminous phase like that observed at low redshift in the 1 Jy ULIRGs. A more physically meaningful test of this scenario would be to compare the environment of local QSOs with the environment of $z \geq 0.5$ ULIRGs to take into account the finite duration of the ULIRG-QSO evolutionary sequence. The recent environmental studies of distant ULIRGs by Blain et al. (2004) and Farrah et al. (2004, 2006) indeed point to slightly richer environments, which more strongly resemble the environments of the QSOs from McLure & Dunlop.

A posteriori, the distinct high- B_{gc} tail in the distribution of the QSOs of McLure & Dunlop (2001) is not unexpected given the host properties of these particular QSOs: ~ 4 – 5 times larger host sizes and luminosities relative to the 1 Jy ULIRGs (Dunlop et al. 2003; Veilleux et al. 2002, 2006). More luminous hosts live in richer environments on average than hosts of lower luminosity. As pointed out by Veilleux et al. (2006) and Dasyra et al. (2007), the hosts of the QSOs from the Palomar-Green sample (these QSOs are less radio and X-ray luminous than the QSOs of McLure & Dunlop 2001) are a better match in host size and luminosity to the local ULIRGs. This may explain the generally better (although not

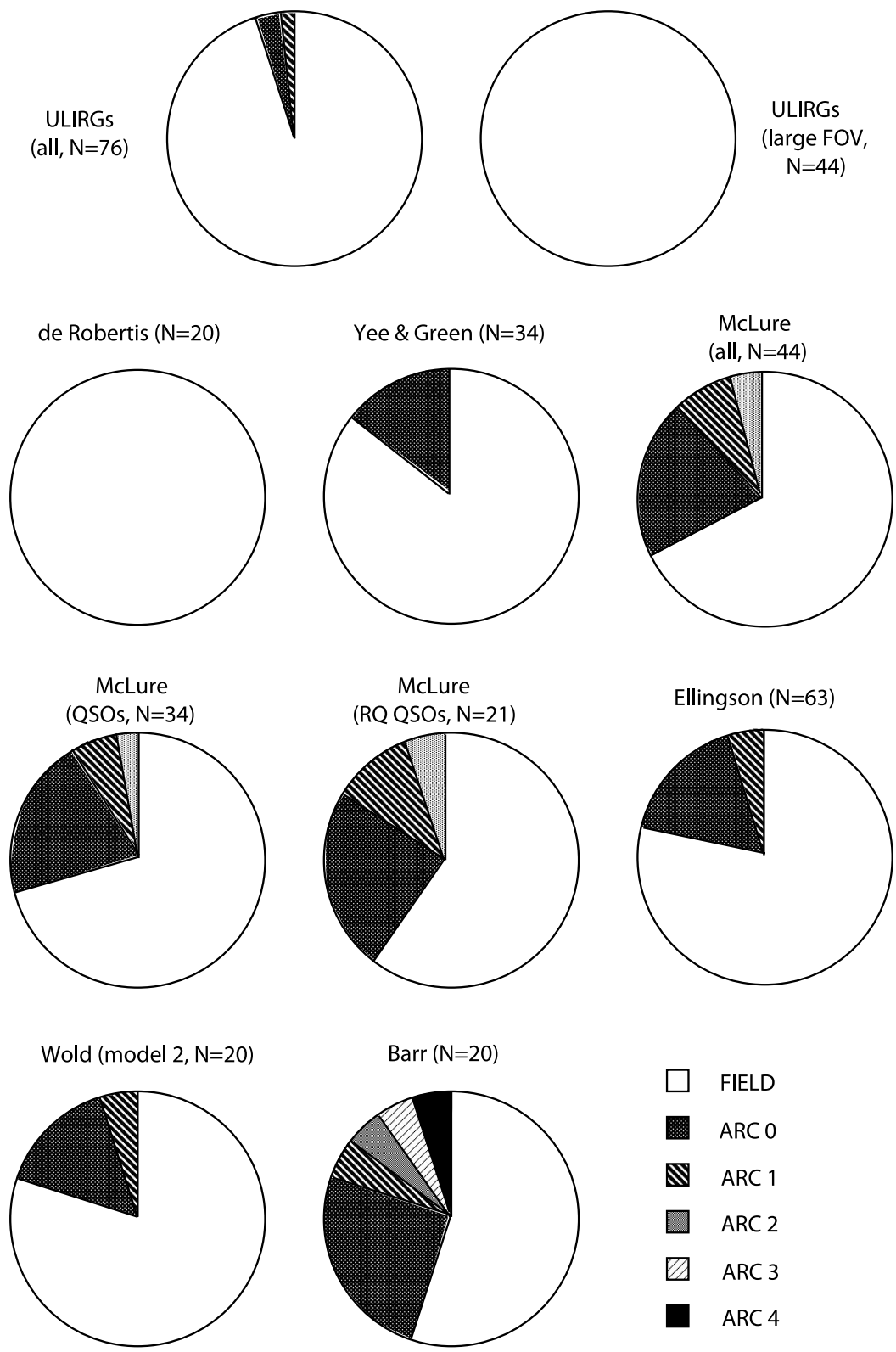


FIG. 6.—Pie-chart diagrams showing the distributions of environment richness parameters typical of field galaxies and clusters of Abell richness classes 0–4 for the 11 different samples considered in this paper. See caption to Fig. 5 for a description of these samples. The results of statistical comparisons between these various data sets are listed in Table 2. None of these data sets appears to be drawn from the same parent population as the local ULIRGs, although considerable overlap in the values of the environmental richness parameters is seen between the various samples, particularly the local ULIRGs (this paper), local Seyferts (de Robertis et al. 1998b), and PG QSOs (Yee & Green 1984).

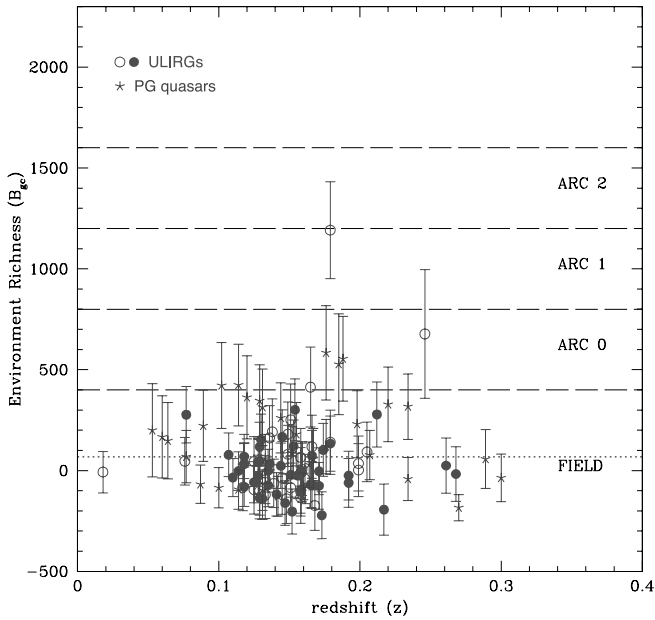


FIG. 7.—Comparison of the environment richness parameter for the local ULIRGs with the $z \approx 0.2$ PG QSOs of Yee & Green (1984). The meaning of the horizontal lines and open and filled circles is the same as that in Fig. 1. There is considerable overlap in the B_{gc} distributions of local ULIRGs and PG QSOs, although a statistical analysis between these two sets of objects generally indicates that they are not drawn from the same parent population. [See the electronic edition of the Journal for a color version of this figure.]

perfect) agreement between the environments of PG QSOs and 1 Jy ULIRGs.

5.3. Intermediate-Redshift QSOs

For the sake of completeness, we display in Figures 5, 6, and 9 the results from our study of local ULIRGs alongside the results

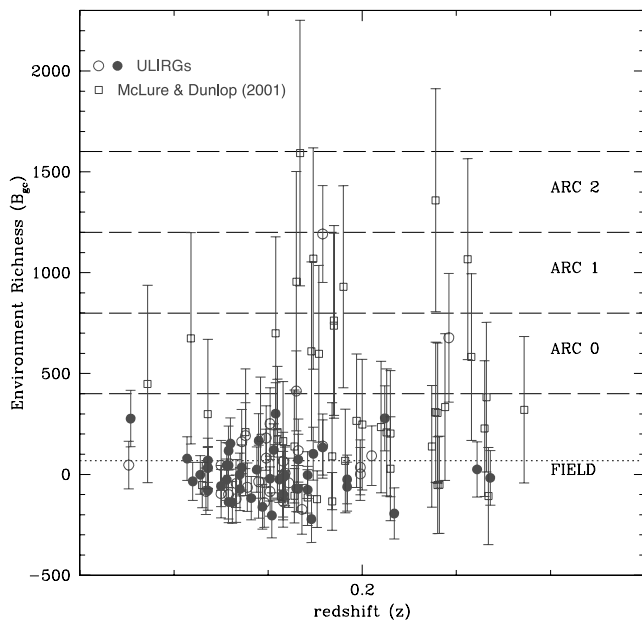


FIG. 8.—Comparison of the environment richness parameter for the local ULIRGs with the $z \approx 0.2$ radio-quiet and radio-loud QSOs of McLure & Dunlop (2001; the radio galaxies are not shown). The meaning of the horizontal lines and open and filled circles is the same as that in Fig. 1. The environment of these QSOs is distinctly richer on average to that of the local ULIRGs, as confirmed in general by a more rigorous statistical analysis. [See the electronic edition of the Journal for a color version of this figure.]

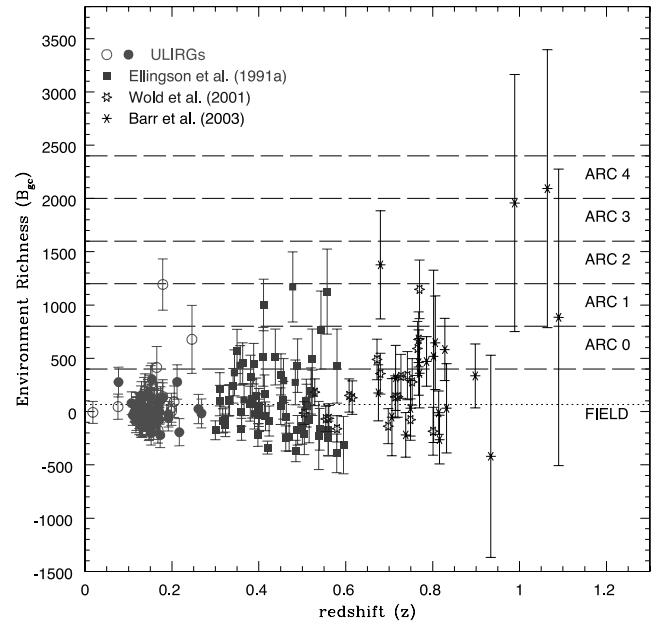


FIG. 9.—Comparison of the environment richness parameter for the local ULIRGs with the $0.3 < z < 0.6$ radio-loud and radio-quiet QSOs of Ellingson et al. (1991), the $0.5 \leq z \leq 0.8$ radio-quiet QSOs of Wold et al. (2001), and the $0.6 < z < 1.1$ radio-loud QSOs of Barr et al. (2003). The meaning of the horizontal lines and open and filled circles is the same as that in Fig. 1. The B_{gc} distributions of these QSOs overlap considerably with that of the local ULIRGs, despite the significant difference in redshifts. [See the electronic edition of the Journal for a color version of this figure.]

presented by Ellingson et al. (1991), Wold et al. (2001), and Barr et al. (2003) for 63 radio-quiet and radio-loud QSOs at $0.3 < z < 0.6$, 20 radio-quiet QSOs at $0.5 \leq z \leq 0.8$, and 20 radio-loud QSOs at $0.6 < z < 1.1$, respectively. All three groups use the same basic method outlined in § 3 to calculate the spatial correlation amplitude, and all groups assume the same value for H_0 . However, Ellingson et al. (1991) assume $q_0 = 0.02$ instead of 0.5 ($\Omega_m = 0.04$ instead of 1, if $\Omega_\lambda = 0$). There is no simple way to scale the B_{gc} -values for different cosmological models (other than H_0) since its computation is rather complicated (§ 3), so Figures 5, 6, and 9 show the B_{gc} -values corrected for the different H_0 but not the different Ω_m . Once again, we see considerable overlap between the various distributions, but the statistical analysis formally rules out that they come from the same parent population (Table 2). The amount of overlap in B_{gc} -values is quite remarkable given the difference in redshifts between the various samples. These results further support a connection between ULIRGs and some QSOs.

6. CONCLUSIONS

We have derived the spatial cluster-galaxy correlation amplitude, B_{gc} , for 76 $z < 0.3$ ULIRGs from the 1 Jy sample and compared our results with those in the literature on $z < 0.05$ AGNs, $z \approx 0.2$ QSOs, and $0.3 \lesssim z \lesssim 1$ QSOs. The main results are as follows:

1. Local ULIRGs live in environments which are similar on average to that of field galaxies. However, there are a few exceptions: some objects apparently lie in clusters of Abell classes 0 and 1.
2. The infrared luminosity, optical spectral type, and *IRAS* 25 to 60 μm flux ratios of ULIRGs show no dependence with environment.

3. The ULIRG environment does not vary systematically over the redshift range covered by our sample (mostly $0.1 < z < 0.22$).

4. There is a lot of overlap between the B_{gc} distribution of local ULIRGs and those of local Seyferts, local QSOs, and intermediate- z QSOs. However, quantitative statistical comparisons show that the various B_{gc} distributions are not drawn from the same parent population. The average environment of ULIRGs appears to be intermediate between that of local Seyferts and local QSOs. Local ULIRGs show a broader range of environments than local Seyferts, which are exclusively found in the field. The B_{gc} distribution of QSOs show a distinct tail at high values that is not seen among local ULIRGs. This slight environmental discrepancy between local QSOs and ULIRGs is not unexpected: recent morphological studies have found that some of the more radio and X-ray luminous local QSOs used in this comparison have more luminous and massive hosts than local ULIRGs. A better match in host and environmental properties is seen when the comparison is made with the PG QSOs.

5. Overall, the results of this study suggest that ULIRGs can be a phase in the lives of all types of AGNs and QSOs, but not all moderate-luminosity QSOs may have gone through a ULIRG phase. Published studies of the environments of more distant ULIRGs, perhaps the actual predecessors of the local QSOs we see today, provide further support for an evolutionary connection between ULIRGs and QSOs.

We thank D. C. Kim for his help in organizing the data set used for this paper. B. A. Z. and S. V. acknowledge partial support of this research by a National Science Foundation (NSF) CAREER grant AST 98-74973 and NASA grant 1263752 issued by the Jet Propulsion Laboratory, California Institute of Technology. This research has made use of the NASA/IPAC Extragalactic Database (NED), which is operated by the JPL, Caltech, under contract with NASA.

REFERENCES

- Andersen, V., & Owen, F. 1994, *AJ*, 108, 361
 Barnes, J. E. 2004, *MNRAS*, 350, 798
 Barr, J. M., Bremer, M. N., Baker, J. C., & Lehnert, M. D. 2003, *MNRAS*, 346, 229
 Blain, A. W., Chapman, S. C., Smail, I., & Ivison, R. 2004, *ApJ*, 611, 725
 Chapman, S. C., Blain, A. W., Smail, I., & Ivison, R. J. 2005, *ApJ*, 622, 772
 Croom, S. M., et al. 2005, *MNRAS*, 356, 415
 Dasyra, K., et al. 2006a, *ApJ*, 638, 745
 ———. 2006b, *ApJ*, 651, 835
 ———. 2007, *ApJ*, 657, 102
 Davis, M., & Peebles, P. J. E. 1983, *ApJ*, 267, 465
 de Robertis, M. M., Hayhoe, K., & Yee, H. K. C. 1998a, *ApJS*, 115, 163
 de Robertis, M. M., Yee, H. K. C., & Hayhoe, K. 1998b, *ApJ*, 496, 93
 Downes, D., & Solomon, P. M. 1998, *ApJ*, 507, 615
 Dunlop, J. S., McLure, R. J., Kukula, M. J., Baum, S. A., O’Dea, C. P., & Hughes, D. H. 2003, *MNRAS*, 340, 1095
 Ellingson, E., Yee, H. K. C., & Green, R. F. 1991, *ApJ*, 371, 49
 Farrah, D., et al. 2004, *MNRAS*, 349, 518
 ———. 2006, *ApJ*, 641, L17
 Genzel, R., Tacconi, L. J., Rigopoulou, D., Lutz, D., & Tecza, M. 2001, *ApJ*, 563, 527
 Genzel, R., et al. 1998, *ApJ*, 498, 579
 Gladders, M. D., & Yee, H. K. C. 2005, *ApJS*, 157, 1
 Groth, E. J., & Peebles, P. J. E. 1977, *ApJ*, 217, 385
 Hill, G. J., & Lilly, S. J. 1991, *ApJ*, 367, 1
 Hughes, D. H., et al. 1998, *Nature*, 394, 241
 Kauffmann, G., et al. 2004, *MNRAS*, 353, 713
 Kim, D.-C., & Sanders, D. B. 1998, *ApJS*, 119, 41
 Kim, D.-C., Veilleux, S., & Sanders, D. B. 1998, *ApJ*, 508, 627
 ———. 2002, *ApJS*, 143, 277
 Kron, R. G. 1980, *ApJS*, 43, 305
 Longair, M. S., & Seldner, M. 1979, *MNRAS*, 189, 433
 Lonsdale, C. J., Farrah, D., & Smith, H. 2006, *Astrophysics Update 2*, ed. J. W. Mason (New York: Springer), 303
 Lutz, D., Veilleux, S., & Genzel, R. 1999, *ApJ*, 517, L13
 Lutz, D., et al. 1998, *ApJ*, 505, L103
 Martin, C. L. 2005, *ApJ*, 621, 227
 McLure, R. J., & Dunlop, J. S. 2001, *MNRAS*, 321, 515
 Mihos, J. C., & Hernquist, L. 1996, *ApJ*, 464, 641
 Miller, C. J., Nichol, R. C., Gómez, P. L., Hopkins, A. M., & Bernardi, M. 2003, *ApJ*, 597, 142
 Rigopoulou, D., Spoon, H. W. W., Genzel, R., Lutz, D., Moorwood, A. F. M., & Tran, Q. D. 1999, *AJ*, 118, 2625
 Rupke, D. S., Veilleux, S., & Sanders, D. B. 2002, *ApJ*, 570, 588
 ———. 2005a, *ApJS*, 160, 115
 ———. 2005b, *ApJ*, 632, 751
 Sanders, D. B., & Mirabel, I. F. 1996, *ARA&A*, 34, 749
 Sanders, D. B., et al. 1988, *ApJ*, 325, 74
 Schmidt, M., & Green, R. F. 1983, *ApJ*, 269, 352
 Scoville, N. Z., et al. 2000, *AJ*, 119, 991
 Seldner, M., & Peebles, P. J. E. 1978, *ApJ*, 225, 7
 Serber, W., Bahcall, N., Ménard, B., & Richards, G. 2006, *ApJ*, 643, 68
 Smail, I., Ivison, R. J., & Blain, A. W. 1997, *ApJ*, 490, L5
 Söchting, I. K., Clowes, R. B., & Campusano, L. E. 2004, *MNRAS*, 347, 1241
 Soifer, B. T., et al. 2000, *AJ*, 119, 509
 ———. 2001, *AJ*, 122, 1213
 Surace, J. A., & Sanders, D. B. 1999, *ApJ*, 512, 162
 Surace, J. A., Sanders, D. B., & Evans, A. S. 2001, *AJ*, 122, 2791
 Tacconi, L. J., et al. 2002, *ApJ*, 580, 73
 Tran, Q. D., et al. 2001, *ApJ*, 552, 527
 Veilleux, S., Cecil, G., & Bland-Hawthorn, J. 2005, *ARA&A*, 43, 769
 Veilleux, S., Kim, D.-C., & Sanders, D. B. 1999a, *ApJ*, 522, 113
 ———. 2002, *ApJS*, 143, 315
 Veilleux, S., Sanders, D. B., & Kim, D.-C. 1997, *ApJ*, 484, 92
 ———. 1999b, *ApJ*, 522, 139
 Veilleux, S., et al. 2006, *ApJ*, 643, 707
 Wake, D. A., et al. 2004, *ApJ*, 610, L85
 Waskett, T. J., Eales, S. A., Gear, W. K., McCracken, H. J., Lilly, S., & Brodwin, M. 2005, *MNRAS*, 363, 801
 Wold, M., Lacy, M., Lilje, P. B., & Serjeant, S. 2000, *MNRAS*, 316, 267
 ———. 2001, *MNRAS*, 323, 231
 Yee, H. K. C. 1991, *PASP*, 103, 396
 Yee, H. K. C., & Ellingson, E. 2003, *ApJ*, 585, 215
 Yee, H. K. C., & Green, R. F. 1984, *ApJ*, 280, 79
 ———. 1987, *ApJ*, 319, 28
 Yee, H. K. C., Green, R. F., & Stockman, H. S. 1986, *ApJS*, 62, 681
 Yee, H. K. C., & López-Cruz, O. 1999, *AJ*, 117, 1985